Phys Chem Minerals (2003) 30: 31 – 38
DOI 10.1007/s00269-002-0279-x

ORIGINAL PAPER

S. K. Deb · M. H. Manghnani · K. Ross
R. A. Livingston · P. J. M. Monteiro

Raman scattering and X-ray diffraction study of the thermal decomposition of an ettringite-group crystal

Received: 9 July 2001 / Accepted: 14 August 2002

Abstract A Raman scattering and X-ray diffraction study of the thermal decomposition of a naturally occurring, ettringite-group crystal is presented. Raman spectra, recorded with increasing temperature, indicate that the thermal decomposition begins at ≈55 °C, accompanied by dehydration of water molecules from the mineral. This is in contrast to previous studies that reported higher temperature breakdown of ettringite. The dehydration is completed by 175 °C and this results in total collapse of the crystalline structure and the material becomes amorphous. The Raman scattering results are supported by X-ray diffraction results obtained at increasing temperatures.

Keywords Ettringite · Raman scattering · X-ray diffraction · Thermal decomposition · Dehydration

S. K. Deb (✉) · M. H. Manghnani
Hawaii Institute of Geophysics and Planetology,
University of Hawaii at Manoa, Honolulu,
Hawaii 96822, USA

K. Ross
Department of Geology and Geophysics,
University of Hawaii at Manoa, Honolulu,
Hawaii 96822, USA

R. A. Livingston
Federal Highway Administration,
6300 Georgetown Pike, McClean Virginia 22101, USA

P. J. M. Monteiro
Department of Civil and Environmental Engineering,
University of California, Berkeley,
California 94720, USA

Present address: S. K. Deb
Synchrotron Radiation Section,
Bhabha Atomic Research Center, Mumbai 400085, India
e-mail: skdeb@apsara.barc.ernet.in
Fax: +091-22-5505151
Tel.: +091-22-5595038

Introduction

Ettringite is a complex mineral of hydrated calcium aluminosulfate with the chemical formula $Ca_6[Al(OH)_6]_2(SO_4)_3{\cdot}xH_2O$ with $x \approx 26$. Ettringite is found very rarely in nature and was originally discovered as transparent acicular crystals lining the cavities of metamorphosed limestone inclusions in leucite-nepheline-tephrite from Ettringer-Bellerberg near the village of Ettringen (Bannister et al. 1936). It has gained considerable attention due to its role in the long-term deterioration of concrete structures exposed to sulfate attack. Ettringite is formed during the initial stages of hydration of Portland cement containing small amounts of gypsum as a source of soluble sulfate; however, as gypsum is consumed, most of the ettringite transforms to aluminium monosulfate hydrate. The equilibrium between ettringite and monosulfate hydrate is stable for concrete not exposed to external sources of sulfate. In marine structures or structures in contact with groundwater containing high levels of sulfate, the monosulfate hydrate reverts back to ettringite, causing expansion and cracking of the structure (Mehta and Monteiro 1993). The precipitation of ettringite in the early stages of hydration does not lead to cracking because the cement paste matrix is porous and flexible, but when ettringite forms at later stages the matrix is rigid and brittle and cannot accommodate the expansion. The significance of ettringite in cement and concrete durability is reviewed in detail by Taylor (1990). Ettringite can be synthesized in the laboratory by a number of different procedures (Hasset et al. 1990; Atkins et al. 1992). It normally crystallizes as prismatic needles (c axis) of high aspect ratio and hexagonal cross-section. However, different morphologies have been observed for growth with organic additives (Pöllmann et al. 1990). Its crystallographic structure was first investigated by Bannister et al. (1936), and the space group was determined to be $P6_3/mmc$ with $Z = 2$ and $a = 1.126$ nm and $c = 2.148$ nm. Moore and Taylor (1968) had supported

this structure initially; however, in a later paper (Moore and Taylor 1970) they reported that the actual structure is trigonal with space group $P31c$. The apparent hexagonal symmetry of some crystals was attributed to twinning. They showed that the crystal structure is based on columns in hexagonal array running parallel to the prism (c) axis, with the SO_4 anions and H_2O molecules in the intervening channels. The columns are of empirical formula $[Ca_3Al(OH)_6{\cdot}12H_2O]_2^{3+}$ and are composed of $Al(OH)_6$ octahedra alternating with triangular groups of edge-sharing CaO_8 polyhedra with which they share the $(OH)^-$ ions. Each Ca ion is coordinated to four H_2O molecules, the hydrogen atoms of which form a column of nearly cylindrical surface. For each channel, there are two SO_4 tetrahedra pointing up, followed by one pointing down, and then followed by a site containing three water molecules. This site is only partially occupied so that there are only two water molecules present at any time. The repeat distance along the c axis is 1.07 nm. The positions of the heavy ions were determined from X-ray diffraction (XRD) (Moore and Taylor 1970) and the locations of the H ions on the hydroxyl groups and orientation of the water molecules were determined by Berliner (1998) using neutron diffraction with hydrogen replaced by deuterium.

The ettringite structure can accommodate substitution of both the anions and cations and this structure has come to be used in a generic sense to represent the AFt phase, where $A \Rightarrow Al_2O_3$, $F \Rightarrow Fe_2O_3$ and $t \Rightarrow$ trisulfate. Complex hydrates belonging to the ettringite structure tend to be fragile and easily decompose on heating to the AFm phase where $m \Rightarrow$ monosulphate, accompanied by dehydration. The thermal decomposition of ettringite has been reported to occur at 120 °C by thermal analysis (Taylor 1990) whereas an XRD and FTIR study (Hall et al. 1996) has reported a temperature of 114 °C in a slurry made up of ettringite and water contained in a sealed capsule. The XRD study indicates sudden decomposition at 114 °C and the principal ettringite reflections are replaced by new ones, which were identified with those corresponding to the monosulfate phase. On the other hand, it was shown by the weight loss curve (Taylor 1990) that ettringite begins to lose water rapidly at about 50 °C under ambient conditions. Upon decomposition, ettringite is considered to transform into calcium aluminomonosulfate and gypsum or bassanite together with release of interstitial water molecules (Hall et al. 1996).

It is known that Cr, Mn, Fe and Si all are capable of substitution on the Al site in the ideal ettringite formula (Hawthorne et al. 2000). Further, CO_3 can substitute on the SO_4 site and when this happens, the solid solution is known as thaumasite $[Ca_3Si(CO_3)(SO_4)(OH)_6{\cdot}12H_2O]$ or jouravskite $[Ca_6Mn_2(SO_4, CO_3)_3(OH)_{12}{\cdot}24H_2O]$. When the $B(OH)_4$ group substitutes for SO_4, the mineral is called sturmanite $\{[Ca_6(Fe,Mn,Al)_2(SO_4)_2(B(OH)_4](OH)_{12}{\cdot}26H_2O\}$ or charlesite. Sturmanite belongs to the same crystal space group $P31c$ as ettringite, whereas thaumasite belongs to $P6_3/m$ (Roberts et al. 1990). However, the powder XRD pattern of all these minerals is very similar with similar d spacing, except for a slight difference in relative intensities of different reflections. This makes it very difficult to characterize these minerals except by high-resolution powder XRD with full Reitvelt refinement (Barnett et al. 1999). All these related structures mentioned above can be classified as ettringite-group minerals.

The water molecules in hydrated minerals play a significant role in determining the interaction between the other structural units in the mineral, and different types of transitions in these minerals depend to a large extent on the details of these interactions. The dehydration of water molecules from these minerals therefore influences the thermodynamic properties and occurrence of structural change in them. In this paper, we report a Raman scattering and X-ray diffraction (XRD) study of the thermal dehydration/decomposition of an ettringite-group crystal, based on changes observed in the Raman spectrum and XRD pattern as a function of temperature. We show that the process of dehydration begins at a temperature of ≈53 °C and proceeds very rapidly till about 65 °C. Subsequently, it continues at a slower rate and by 175 °C the crystal loses almost all the water molecules. The Raman scattering observations were supplemented by an X-ray diffraction study of the material before and after dehydration. The final phase of the crystal was found to be X-ray-amorphous and we ascribe this to the complete breakdown of the crystal structure due to loss of water of crystallization. This will have far-reaching implications in the role played by ettringite in the deterioration of cement and concrete structures.

Experimental

The Raman spectra reported in this paper have been recorded from a naturally occurring crystal of ettringite. A detailed chemical, spectroscopic and XRD analysis of the sample is given in the following section. The crystal easily breaks up into long thin needles (a few mm in size) with c axis along the needle axis. The spectra were excited using a 514.5-nm line from a Spectra Physics Ar^+ laser. The sample used for Raman scattering and XRD study was taken from the outer rim of the crystal. Transparent long needle-shaped crystals were selected and the laser power was adjusted to obtain the best signal-to-noise ratio without causing any sample damage by local laser heating. The scattered light was analyzed using a confocal Dilor XY spectrometer with microscope attachment and CCD detection. A Leitz 50X microscope objective was used to focus the laser beam onto the sample as well as to collect the backscattered Raman signal. The crystal was heated on a heating stage in ambient atmosphere and the temperature was controlled to within ±1 °C. All the spectra were recorded without using any polarization analyzer. The powder X-ray diffraction patterns were collected at intervals of 0.02° from 2θ values of 5° to 60° at the scan rate of 2° min^{-1} on a Siemens D-5000 diffractometer equipped with a position-sensitive detector. Two different samples were heated to 70 and 250 °C, respectively, and their XRD patterns were recorded after cooling down to the ambient temperature. Each of these was kept in the oven for more than 24 h before cooling.

Results

Sample analysis

The ettringite sample was obtained from a natural source in South Africa. We have characterized the sample investigated in this study by chemical analysis, IR and Raman spectroscopy and powder XRD. The chemical analysis of the crystal was performed using a CAMECA electron microprobe. The instrument was operated with a beam energy of 15 kV and beam current of 10 nA. The beam diameter was set at ~10 microns. Count times were limited to 20 s on the peak, with 10 s on each background position. These instrument conditions were set to minimize damage that the electron beam can cause to volatile rich materials during the analysis. A troilite (FeS) standard was used to calibrate for sulfur, but the peak position was re-searched on ettringite. A relatively large shift in peak position is found between sulfide and sulfate. The sample is compositionally zoned with an alumina- and silica-rich core, mantled by an asymmetric rim that is enriched in iron and manganese. The sample is sulfur-deficient in both core and rim. Cation contents in the sample are given in Table 1, with locations on the sectioned crystal described in the table.

The chemical analysis of our sample confirms that Al, Fe, Mn and Si all substitute on the Al site in the ideal ettringite formula (Hawthorne et al. 2000) and the Si, Fe and Mn in the sample are present as solid solution and not as some other contaminating phase. In addition, it is known that CO_3 can substitute on the SO_4 site. The deficiency in sulfur in the microprobe analysis indicates that there should be some other anion group in the sample. Since CO_3 is a likely substituting anion group in this mineral, we recorded the IR absorption spectrum of the sample. The powdered sample was mixed uniformly with KBr in 1% concentration and pelletized and the spectrum was recorded in a Bomem DA8 FTIR spectrometer. The spectrum is shown in Fig. 1 and it has a strong peak at 1115 cm^{-1}, which is due to SO_4, and the peaks at 1687 and 3440 cm^{-1} are due to bending and stretching vibration of water molecules. The mode at 3625 cm^{-1} is due to the OH-stretching vibration of the $Al(OH)_6$ unit. All these modes belong to ettringite, and there is an additional peak at 1410 cm^{-1}, which is due to CO_3 stretch (Trezza and Lavat 2001). Hydroxyl groups can also substitute for SO_4 and some of the sulfur deficiency could be explained by this substitution (Myneni et al. 1998a, b; Myneni 2000). In summary, the sample has a sturmanite (ferric-iron-bearing ettringite analogue) rich "rim", and an ettringite-rich "core", and also has solid solution of other ettringite-group minerals throughout.

We also collected powder X-ray diffraction patterns of the sample and the three most intense reflections correspond to *d* spacings of 9.69 Å (100), 5.59 Å (90) and 3.88 Å (40), respectively. The quantities in brackets are the relative intensities. The corresponding reflections for ettringite are 9.65 Å (100), 5.58 Å (80), 3.88 Å (60) and for its two related structures sturmanite and thaumasite are 9.67 Å (100), 3.89 Å (70), 5.58 Å (70) and 9.56 Å (100), 5.51 Å (40) and 3.41 Å (20), respectively. Thus, the average structure of the mineral is more like ettringite and sturmanite rather than thaumasite. The JCPDS database also lists another mineral, once known as woodfordite $[Ca_6Al_2(SO_4,SiO_4,CO_3)_3(OH)_{12}{\cdot}26H_2O]$ and now classified as an ettringite analogue, which has a similar diffraction pattern. In fact, the *d* spacing and intensity ratio matches best with this mineral. Thus, the compositional, IR and XRD characterization of the mineral indicates that it is not a stoichiometric ettringite compound but a solid solution of this group of minerals, with considerable compositional variation between rim and core.

Assignment of Raman modes

The space group of ettringite crystal is $P31c$ with two formula units per unit cell (Berliner 1998). We concentrate on the changes occurring in the Raman spectra corresponding to the internal vibrations of SO_4 ions, $Al(OH)_6$ units and different water molecules and the

Table 1 Electron microprobe analysis of the sample. The Ca has been set at 6 and the composition of the rest of the atoms has been shown relative to Ca. The composition analysis for samples taken from different positions of the sample are shown in the *left column*. The positions have been divided into *rim* and *core*

Position	(Al + Fe + Mn + Si)	Al	Si	S	Ca	Mn	Fe
30 μm from edge	2.08	0.42	0.18	2.19	6	0.36	1.13
0.4 mm from edge	1.91	0.33	0.15	2.46	6	0.27	1.16
0.65 mm from edge	1.9	0.32	0.17	2.41	6	0.33	1.09
0.7 mm from edge	1.84	0.35	0.18	2.4	6	0.28	1.04
0.8 mm from edge	1.81	0.53	0.18	2.45	6	0.24	0.87
0.2 mm from edge	2.02	0.43	0.15	2.26	6	0.26	1.1
Mean rim	1.93	0.40	0.17	2.36	6	0.3	1.06
Core 1	2.17	1.39	0.57	2.17	6	0.02	0.19
Core 2	2.09	1.35	0.55	2.19	6	0.01	0.19
Core 3	2.05	1.32	0.53	2.15	6	0.01	0.19
Core 4	2.14	1.48	0.51	2.2	6	0.01	0.14
Mean core	2.1	1.38	0.55	2.17	6	0.01	0.18

symmetry character of all the Raman-active modes can be worked out using the group theoretical correlation method. However, we do not intend to perform any polarized Raman measurements to identify the symmetry character of the different modes, and hence the details are not given.

The Raman spectrum of a thin platelet of ettringite crystal taken from the rim is shown in Fig. 2. Here, the *c* axis is normal to the incident and the backscattered light. This figure shows the spectra over 100 to 1250 cm^{-1} containing the internal modes of the SO_4 and Al–$(OH)_6$ units and a few relatively higher-frequency external (rotation and translation) modes. Although there are a large number of Raman-active modes corresponding to the internal modes of SO_4 and Al–$(OH)_6$ units, only a few of the allowed modes are observed in the experimental spectra and this may be due to the very small frequency differences between the correlation split components belonging to a particular type of vibration which makes it very difficult to resolve. Further, it is quite difficult to assign unambiguously the different observed modes in the absence of polarized Raman spectra. However, the vibration character of many of these modes can be identified from the characteristic frequencies of these units. The fundamental Raman frequencies of free SO_4 ion are 981 cm^{-1}(v_1), 451 cm^{-1}(v_2), 1104 cm^{-1}(v_3) and 613 cm^{-1}(v_4) (Berenblut et al. 1973). Since the site and crystal symmetry of the SO_4 ions are lower than the free state symmetry, each of these modes splits up in the crystal. The modes at 416 and 449 cm^{-1} thus belong to the v_2 and those at 581 and 605 cm^{-1} belong to the v_4 types of vibrations of the SO_4 ion. The strongest mode at 988 cm^{-1} belongs to the totally symmetric v_1 mode and the one at 1114 cm^{-1} belongs to the v_3 vibration. The modes at 527 and 551 cm^{-1} could be assigned to the stretching modes of the Al–$(OH)_6$ unit based on a knowledge of the corresponding frequencies in Sn–$(OH)_6$ and Al–$(H_2O)_6$ The Sn–OH-stretching vibrations in $K_2[Sn(OH)_6]$ are at 492 and 520 cm^{-1} (Kolditz and Priess 1963), respectively. Similarly, the symmetric stretching frequencies v_1 (M–OH_2) in $M(OH_2)_6$ units (where M stands for different metal ions) in several alums were reported to lie between 500 and 550 cm^{-1} (Beattie and Best 1997). The Al–O-stretching vibrations in $Al(OH_2)_6$ units in RbAl $(SO_4)_2.12H_2O$ have also been reported at 535 and 530 cm^{-1} (Suresh et al. 1996). Since the molecular weights of OH_2 and OH are very close, we can assume that the symmetric stretching mode in $Al(OH)_6$ will lie in this range.

The Raman spectrum in the range from 3000 to 3750 cm^{-1} covering the O–H-stretching frequency region of water molecules and the OH ions in Al–$(OH)_6$ is shown in Fig. 3. The sharp band at 3624 cm^{-1} is attributed to O–H stretch by comparing this value with those for $Ca(OH)_2$ and $Mg(OH)_2$. The frequency for the O–H-stretching band for $Ca(OH)_2$ and that for

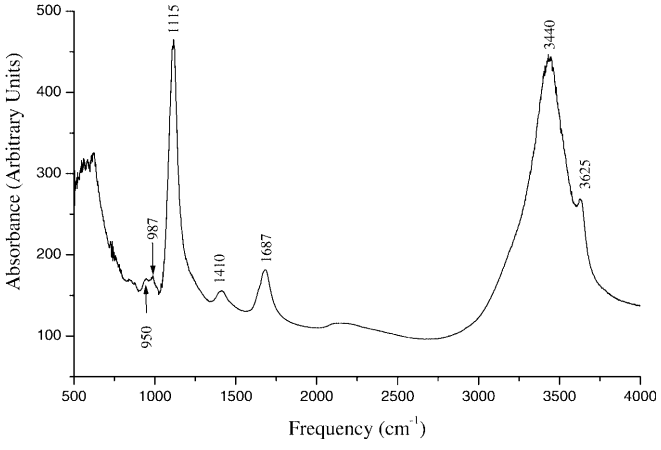

Fig. 1 The IR absorption spectrum of the sample in KBr pellet over the range 500–4000 cm^{-1}

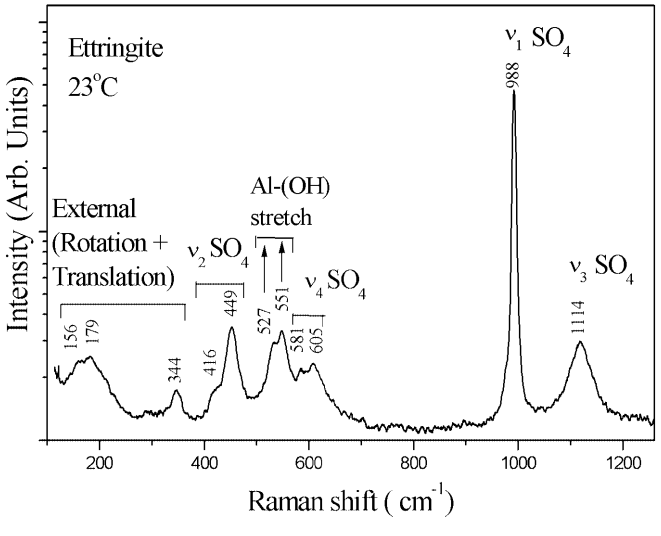

Fig. 2 Raman spectrum of ettringite over the internal modes of SO_4 and $Al(OH)_6$ at 23 °C. The intensity is shown in logarithmic scale to highlight the low intensity peaks. The frequencies of the v_1, v_2, v_3 and v_4 vibrations and also the Al–(OH) stretch vibrations are shown

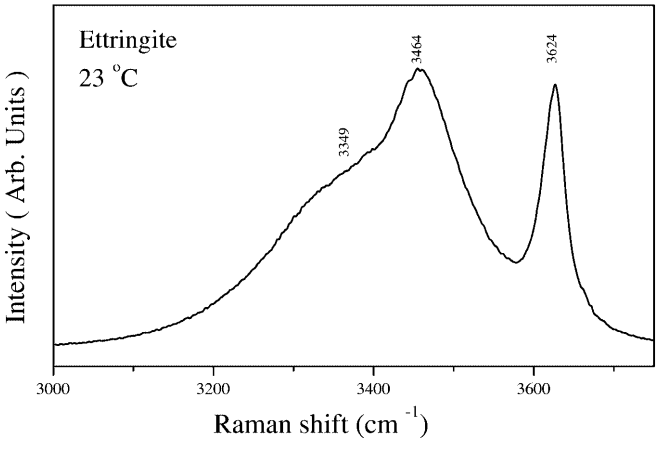

Fig. 3 Raman spectrum of stretching vibration of water and OH ions at 23 °C

$Mg(OH)_2$ have been reported to be at 3618 and 3655 cm^{-1} (Kruger et al. 1989), respectively. The Raman spectrum of the symmetric stretching band of the water molecule is quite strong and broad, with large asymmetry towards the low frequency. The peak position corresponding to this mode for free water is 3707 cm^{-1}, but in solids its value can be lowered as a result of the presence of hydrogen bonding. The broad spectrum with peak at 3464 cm^{-1} and a broad hump at 3349 cm^{-1} are therefore assigned to the stretching vibrations of water molecule. A shift ≈350 cm^{-1} indicates presence of some hydrogen bonding (Novak 1974). It is also known from the crystal structure of ettringite that some of the water molecules occupy the channel sites and the rest of them are coordinated to the Ca ions along the column. The two peaks may therefore be due to the different stretching vibration frequencies corresponding to the water molecules occupying the different sites in the crystal.

The Raman spectrum of ettringite was earlier reported by Myneni et al. (1998a) on a synthetic, stoichiometric ettringite. Their spectrum for symmetric stretch vibration for SO_4 at 990 cm^{-1} differs quite significantly from ours. We observe a sharp line at 988 cm^{-1} whereas they observe three lines at 996, 1008 and 1016 cm^{-1}. They assign these three lines as arising due to different S–O bond distances in SO_4 ions occupying three crystallographically different sites in the unit cell of ettringite. The difference with our spectrum can arise due to the difference in the sample used by Myneni et al. (1998a) and by us. Our sample is highly sulfur-deficient and the balance of the sulfate sites are occupied by CO_3 ions, and also possibly by OH or SiO_4 ions. The Si content of the sample used for Raman spectrum is less than 10% of sulfur content (see Table 1) and that may be the reason why we do not see any Si–O-related Raman lines either in tetrahedral or octahedral coordination in the Raman spectrum of our sample. Myneni et al. (1998a) have shown that the intensity of high-frequency components (at 1008 and 1016 cm^{-1}) is suppressed when SO_4 ions are replaced by 2% AsO_4 ions. Similarly, it is known that in thaumasite the sites between the $[Ca_3Si(OH)_6{\cdot}12\ H_2O]^{4+}$ columns are occupied by CO_3 and SO_4 ions and the Raman spectrum of thaumasite shows a single line at 990 cm^{-1} (Brough and Atkinson 2001). Thus, the presence of CO_3 ions in these sites has a very large influence on the S–O bond distances in ettringite-related minerals, which could give rise to a more or less single value of the S–O distance. This will result in a single Raman line corresponding to the symmetric stretch vibration of SO_4, as was seen in this study. Although there is a considerable amount of CO_3 present in the sample, we do not see the Raman line corresponding to the symmetric stretching vibration of CO_3, perhaps because this mode at 1080 cm^{-1} is masked by the broad asymmetric stretch SO_4 mode at 1114 cm^{-1}

Myneni et al. (1998a) do not show Raman spectra in the water-stretching region; however, their IR spectrum in this range shows a very broad feature ranging from 3000–3400 cm^{-1} assigned to OH-stretching vibration of H_2O and another broad feature at 3560 cm^{-1} due to OH coordinated to Al. This agrees with our observation of a very broad Raman peak over the region 3000–3700 cm^{-1}.

Changes in Raman spectra with temperature

The changes in the Raman spectra over the region of internal vibrations of SO_4 and Al–$(OH)_6$ with increase in temperature are shown in Fig. 4. On being heated, there is practically no change in the spectrum to about 50 °C. However, it changes suddenly at ≈53 °C with the totally symmetric $\nu_1(SO_4)$ mode at 988 cm^{-1} acquiring a high-frequency component. The other modes near 450, 550 and 620 cm^{-1}, which were split in their correlation components in the room-temperature phase, suddenly broaden to become single peaks. The band at ≈1114 cm^{-1} also broadens, with its width increasing from 48 to 76 cm^{-1}. In addition, under visual observation the crystal loses its original transparency and appears milky and there is sudden decrease in intensity of almost all the Raman modes. As the temperature is increased, the intensity of the high-frequency component of the 988-cm^{-1} band increases quite rapidly to about 65 °C, after which it becomes a single broad feature. The change in the shape of the 988-cm^{-1} mode is quite interesting. At 53 °C it starts to acquire a high-frequency component at ≈1008 cm^{-1} and the relative intensity of this component increases quite rapidly to 57 °C, and

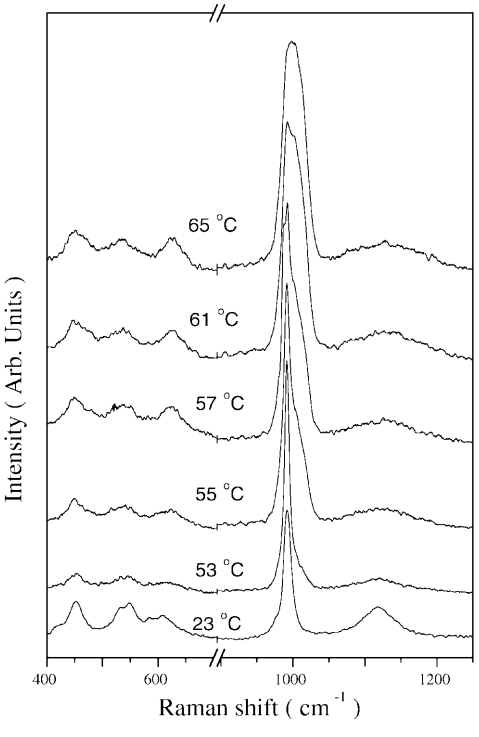

Fig. 4 Raman spectra of the internal modes of SO_4 and $Al(OH)_6$ at different temperatures. The spectra have been broken over 700–900 cm^{-1} and intensity is in logarithmic scale

beyond 61 °C this mode becomes very broad and can no longer be fitted to a combination of the above two components. The spectral changes shown in Fig. 4 take place within a span of about 40 min as the crystal is heated slowly at a constant rate. The temperatures shown are mean temperatures over an acquisition time of about 30 s. The sample used is quite small (about 1 mm in dimension) and kept in the hot spot of the furnace, and we do not expect any significant temperature gradient on the sample and also assume that the sample and oven temperatures are same. The splitting of the v_2, v_4 modes of SO_4 and the Al–OH-stretching mode can be clearly seen before the transition, but they become broad single peaks after the transition.

The stretching mode of water molecules and OH ions also undergoes large changes with increasing temperature, which can be seen in Fig. 5. The spectrum is virtually unchanged to about 50 °C and rapidly changing beyond 53 °C. The water-stretching mode decreases rapidly and by 65 °C the distinct peak at 3450 cm^{-1} and the broad hump at 3250 cm^{-1} disappear and the spectrum consists of the peak at 3600 cm^{-1} with a broad low-frequency asymmetry. The decrease in intensity of the water mode indicates release of water molecules from the crystal and thus the temperature for onset of dehydration is ≈53 °C. It proceeds rapidly till about 65 °C and then slows considerably. Since the intrinsic shape of the stretching mode of water is highly asymmetric, it is difficult to perform any curve-fitting analysis to obtain a quantitative estimate of the water molecules lost by the sample. The relative intensity and position of the band at 3600 cm^{-1} remains essentially the same, indicating that the OH band of the $Al(OH)_6$ remains unchanged. Comparing the changes in the Raman spectra in Figs. 4 and 5, we can correlate the changes in SO_4 and $Al(OH)_6$ internal modes as due mainly to the onset of the dehydration process.

When the sample is cooled from 65 °C to room temperature under ambient condition, the Raman spectrum does not correspond to that for the starting phase of material and remains similar to that obtained at 65 °C. This shows that the transition is irreversible, which is consistent with the fact that the transition is accompanied by dehydration of water from ettringite. If we increase the temperature of the sample above 65 °C there are no significant changes in the spectrum, either over the internal vibration of SO_4 and $Al(OH)_6$ or over the stretching vibration of water and OH ions, and by 175 °C the spectrum in the water-stretching region practically disappears with very little intensity near the OH-stretching region.

XRD patterns taken at different stages of dehydration are shown in Fig. 6. The pattern shown in Fig. 6a is that of the starting material and is very similar to that of ettringite (Satava and Virpek 1975) but shows minor differences due to solid solution. The sharp peaks show that the material is crystalline. The sample was then heated to 70 °C for more than 24 h and the XRD pat-

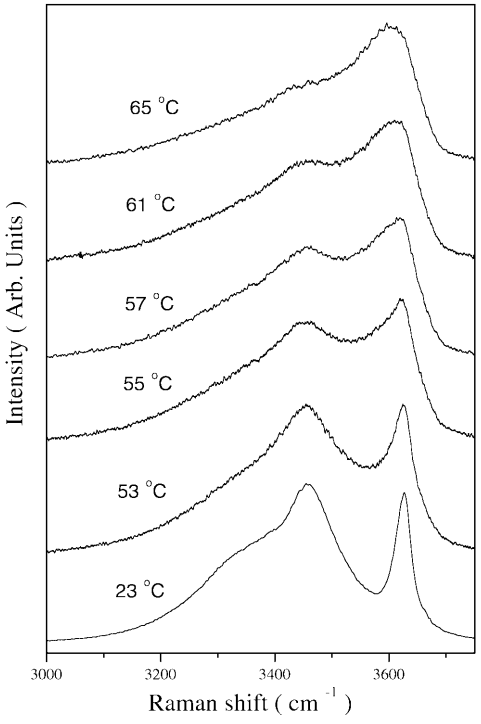

Fig. 5 Raman spectra of water-stretching and OH modes with increasing temperature

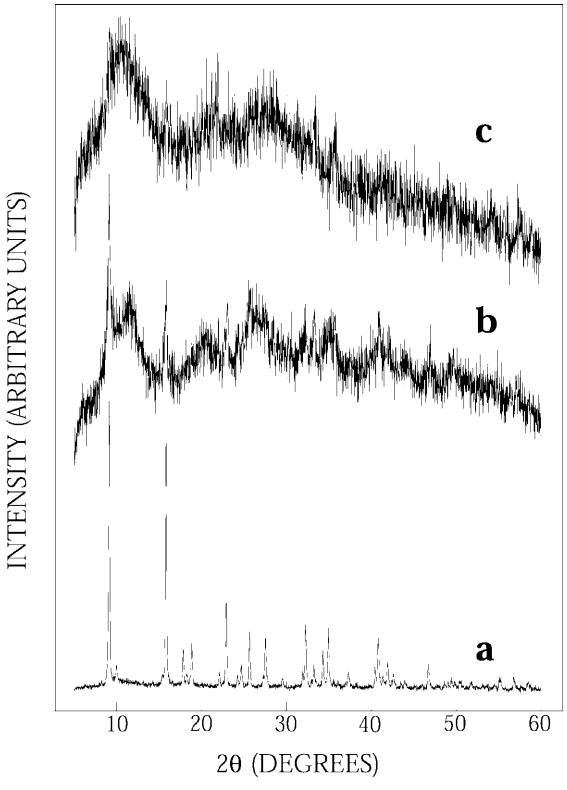

Fig. 6 The XRD pattern recorded at different stages of dehydration: *a* starting sample; *b* the sample heated to 70 °C for 24 h and then cooled to room temperature (22 °C); *c* the sample heated to 200 °C for 24 h and then cooled to room temperature (22 °C)

tern taken after being cooled down to room temperature at ambient condition is shown in Fig. 6b. Almost all the peaks have become broad except the two strongest ones, but we do not see any extra sharp line that would indicate the appearance of any new crystalline material. These observations show that the sample is becoming increasingly disordered due to the loss of water molecules. The pattern shown in Fig. 6c was taken on a sample heated to 200 °C for more than 1 day. It shows that all the peaks have become very broad and the sample has become completely disordered and the XRD pattern is typical of a poorly crystalline/nanocrystalline or an amorphous material.

Discussion

The changes in the Raman spectra of ettringite with increase in temperature show that the spectrum over the internal modes of SO_4, $Al(OH)_6$ and water undergo sudden changes at 53 °C. The changes associated with water vibration modes indicate dehydration of the crystal at the same temperature. An earlier X-ray diffraction and FTIR study (Hall et al. 1996) suggest that ettringite crystal contained in slurry of water decomposes into its monosulfate component and bassanite. However, the Raman spectrum of the v_1 mode of bassanite consists of a strong peak at 1015 cm^{-1} with a "hump" at 1006 cm^{-1}, while that for gypsum consists of a single peak at 1006 cm^{-1}. As has been mentioned earlier, during the initial stages of heating, the v_1 mode could be resolved into two Lorentzian components at 988 and 1008 cm^{-1}. Thus, it is likely that during the initial stage of dehydration, gypsum appears as one of the intermediate/transient components, but not bassanite, in contrast to earlier observations (Hall et al. 1996). However, it has to be stressed that it is difficult to conclude the presence of gypsum solely from the appearance of just one Raman line. The Raman spectrum of the monosulfate phase is not known, and hence it is not possible to identify the other phase unambiguously. Beyond 61 °C all the SO_4 internal modes become very broad and can be represented as the superposition of a large number of components. This reflects considerable disorder in the system with a broad distribution of frequencies for the SO_4 mode originating from a distribution of S–O bond distances and bond angles. We can compare our Raman and XRD data and we observe that above 65 °C the sample is highly disordered and only a very small fraction of the original crystalline material is present after being heated to 70 °C, as can be seen from the presence of a few strong reflections in Fig. 6b. However, we do not see any reflection corresponding to gypsum, indicating that the latter appears only as a transient component during the initial stages of the heating. If we correlate these changes with the changes in the Raman spectrum in the water-stretching region, we can conclude that the dehydration of water molecules from the crystal induces disorder and breakdown of the crystal lattice. Further, on heating the sample to 200 °C, the dehydration is almost complete and the Raman spectrum contains only broad features. Similarly, the XRD pattern shown in Fig. 6c also contains only broad features and this makes the identification of the decomposition products by XRD and Raman scattering practically impossible. Thus, the crystal structure of the mineral is maintained by the presence of the "water of crystallization". The disordered nature of the sample leads to a distribution of bond lengths and bond angles, which results in increase in linewidth of all the Raman lines. Thus our Raman spectrum is consistent with the X-ray data taken after heating the sample to different temperatures.

We also note that the onset of dehydration/decomposition of ettringite takes place at 53 °C in our experiment, whereas Hall et al. (1996) reported a value of 114 °C and Satava and Viprek (1975) quoted a value of 111 °C. This difference can be due to the fact that our sample was heated at ambient atmosphere whereas Hall et al. carried out their measurement in a slurry containing ettringite and water in a sealed capsule. The increased vapour pressure of water in a sealed capsule may prevent the release of water at a lower temperature. Our observations agree with the weight loss measurement, where ettringite begins to lose water rapidly at about 50 °C at ordinary humidity.

Shimoda and Young (2001) reported the structural changes associated with thermal dehydration of ettringite crystals using XRD, thermogravimetry and ^{27}Al NMR. They observed that the crystal loses at most three water molecules below 60 °C, while the loss is very rapid between 60 and 70 °C, losing about 20 molecules within a few hours. Beyond a temperature of 100 °C most of the water molecules are lost within a few minutes. From their XRD and ^{27}Al NMR data, Shimoda and Young (2001) concluded that the crystal retains some long-range order until the Al coordination changes from 6 to 5, after which the short-range order is disrupted and ettringite becomes X-ray-amorphous.

We want to emphasize here that it is difficult to distinguish between an amorphous and a very poorly crystalline phase in XRD. Raman spectra show that the sample is completely dehydrated beyond 175 °C, and if we assume that the sulfate is associated with poorly crystalline Ca or Al sulfate phases, the broad peaks seen in the final XRD should correspond to the most intense reflections of these materials. These reflections for $CaSO_4$ are at 3.50 2.85 and 2.33 Å, and those for $Al_2(SO_4)_3$ are at 3.50, 2.03 and 5.82 Å, respectively. However, the broad peaks seen in Fig. 6c correspond to 8.83, 4.03 and 3.18 Å, respectively, which do not match any of the strong reflections from $CaSO_4$ nor $Al_2(SO_4)_3$. R. van Hoek and Winter (2002) have shown that the XRD patterns of nanocrystalline and amorphous silica are completely different and that the nanocrystalline silica has a broad peak at $2\theta \approx 25°$ while an amorphous silica has a broad peak at $2\theta \approx 20°$. So we feel that the origin of the broad peaks in our material (> 175 °C) is not associated with the poorly crystalline form of any of these compounds but is due to its

"amorphous" nature. Our Raman and XRD results are consistent with each other and also in good agreement with those of Shimoda and Young (2001).

Conclusion

We have reported the Raman spectrum of a naturally occurring crystal of ettringite and investigated its thermal dehydration and decomposition from changes in the Raman spectra with increasing temperature. X-ray diffraction patterns obtained from the material after heating to different temperatures have also been acquired. Our results show that the onset of dehydration and decomposition takes place at a much lower temperature when it is heated under ambient condition, and loses all the water of hydration on being heated to more than 175 °C. Further, the crystal structure of the mineral collapses on losing the water of crystallization and it turns amorphous. This kind of dehydration-induced amorphization of the mineral is in sharp contrast with that in a related material – gypsum. Raman spectroscopy (Sarma et al. 1998) and other studies (Kosztolanyi et al. 1987) indicate that, on being heated, gypsum loses its water of crystallization to transform to bassanite at 388 K and subsequently to anhydrite at 448 K after complete dehydration. However, both the product components are crystalline, exhibiting sharp Raman lines, which is completely different from the final amorphous end product of ettringite.

Acknowledgements This research work was supported by the US Department of Trans-portation, Federal Highway Administration grant no. DTFH61-94-X-00020 to the University of Hawaii. It is a pleasure to thank John Balogh for technical help in experimental work and Dr. Pavel Zinin for many discussions. We would like to thank Dr. G. Ramachandran for help in obtaining the XRD data and Dr. M. N. Deo for help with the IR spectrum.

References

Atkins M, Glasser FP, Kindness A (1992) Cement hydrate phases: solubility at 25 °C 22: 241–246

Bannister FA, Hey M, Bernal JD (1936) Ettringite from Scawt Hill Co. Antrim. Miner Mag 24: 324–329

Barnett SJ, Adam CD, Jackson ARW, Hywel-Evans PD (1999) Identification and characterization of thaumasite by XRD techniques. Cement Concrete Res 21: 123–128

Beattie JK, Best SP (1997) Structures and spectroscopy of hexaaquametal(III) ions. Coord Chem Rev 166: 391–415

Berenblut BJ, Dawson P, Wilkinson GR (1973) Comparison of Raman spectra of anhydrite ($CaSO_4$) and gypsum ($CaSO_4.2H_2O$) Spectrochim Acta 29 A: 29–36

Berliner R (1998) The structure of ettringite. In: Cohen M, Mindess S, Skalny J (eds) Material science of concrete: the sydney diamond symposium, Honolulu, Hawaii, Aug 30–Sept. 3 1998 Am Ceram Soc Westerville, Ohio, pp 127–141

Brough AR, Atkinson A (2001) Micro-Raman spectroscopy of thaumasite. Cement Concrete Res 31: 421–424

Hall C, Barnes P, Billimore AD, Jupe AC, Turrilas X (1996) Thermal decomposition of ettringite $Ca_6[Al(OH)_6]_2(SO_4)_3.26H_2O$. J Chem Soc Faraday Trans 92: 2125–2129

Hasset DJ, McCarthy GJ, Kumarathasan P, Pflughoeft-Hasset D (1990) Synthesis and characterization of selenite and sulfate-selenite ettringite structure phases. Mater Res Bull 25: 1347–1354

Hawthorne FC, Krivovichev SV, Burns PC (2000) The crystal chemistry of sulfate minerals. In: Alpers CN, Jambor JL, Norstrom DK (eds) Reviews in Mineralogy Geochem, vol 40, Sulfate minerals, Mineral Soc Am Washington, DC

Kolditz VL, Priess H (1963) Fluorohydroxokomplexe des Germaniums und Zinns. Z Anorg Allgem Chem 325: 252–262

Kosztolanyi C, Mullis J, Weidmann M (1987) Measurements of the phase transformation temperature of gypsum-anhydrite, included in quartz, by microthermometry and Raman microprobe techniques. Chem Geol. 61: 19–28

Kruger MB, Wlliams Q, Jeanloz R (1989) Vibrational spectra of $Mg(OH)_2$ and $Ca(OH)_2$. J Chem Phys 91: 5910–5915

Mehta PK, Monteiro PJM (1993) Concrete: microstructure, properties and materials. McGraw Hill, New York

Moore AE, Taylor HFW (1968) Crystal structure of ettringite. Nature 218: 1048–1049

Moore AE, Taylor HFW (1970) Crystal structure of ettringite. Acta Crystallogr (B) 26: 386–393

Myneni SCB (2000) X-ray and vibrational spectroscopy of sulfate in geologic materials. In: Alpers CN, Jambor JL, Nordstrom DK (eds) Reviews in Mineralogy Sulfate minerals: crystallography, geochemistry, and environmental significance, vol 40. 113–172. Mineral Soc Am Washington, DC

Myneni SCB, Traina SJ, Waychunas GTA, Logan TJ (1998a) Vibrational spectroscopy of functional group chemistry and arsenate coordination in ettringite. Geochim Cos Acta 21/22: 3499–3514

Myneni SCB, Traina SJ, Logan TJ (1998b) Ettringite solubility and geochemistry of the $Ca(OH)_2$–$Al_2(SO_4)_3$–H_2O system at 1 atm pressure and 298 K. Chem Geol 148: 1–19

Novak A (1974) Hydrogen bonding in solids: correlation of spectroscopic and crystallographic data. In: Dunitz DJ, Hemmerish P, Holm RH, Ibers JA, Jorgensen CK, Neilands JB, Reinen D, Williams RJP (eds) Structure and bonding, vol 18. Springer, Berlin Heidelberg New York, pp 177–216

Pöllmann H, Kuzel HJ, Wenda R (1990) Solid solution of ettringites, part I. Incorporation of OH and CO_3 in $3CaO:Al_2O_3:3CaSO_4:32H_2O$. Cement Concrete Res 20: 941–947

Roberts WL, Campbell TJ, Rapp GR (1990) Encyclopia of mineralogy, 2nd ed. Van Nostrand New York

Sarma LP, Prasad PSR, Ravikumar N (1988) Raman spectroscopic study of phase transitions in natural gypsum. J. Raman Spectrosc. 29: 851–856

Satava V, Viprek O (1975) Thermal decomposition of ettringite under hydrothermal conditions. J Am Ceram Soc 58: 357–359

Shimoda Y, Young JP (2001) Structural changes during thermal dehydration of ettringite. Adv Cement Res 31: 77–81

Suresh G, Ratheesh R, Jayasree RS, Nayar VU, Keresztury G (1996) Infrared and polarized Raman spectra of $RbAl(SO_4)_2{\cdot}12H_2O$. J Sol State Chem 122: 333–337

Taylor HFW (1990) Cement Chemistry. Academic Press, London

Trezza MA, Lavat AE (2001) Analysis of the system $3CaO.Al_2O_3$-$CaSO_4.2H_2O$–$CaCO_3$–H_2O by FT-IR spectroscopy. Cement Concrete Res 31: 869–872

van Hoek ER, Winter R (2002) Amorphous silica and the intergranular structure of nanocrystalline silica. Phys Chem Glass (in press)